Remote Sensing Applications: Society and Environment 42 (2026) 102005

Contents lists available at ScienceDirect

Remote Sensing Applications: Society and Environment

journal homepage: www.elsevier.com/locate/rsase

Urban morphology and the heat island effect in African cities: Evidence from Ghana, Togo, and Tanzania

Stephan Schmidt[a,*], Yucheng Zhang[b], Wenzheng Li[c], Houpu Li[d]

[a] Department of City and Regional Planning, Cornell University, West Sibley Hall, Ithaca, NY, 14853, USA
[b] Department of Urban Planning and Design, The University of Hong Kong, China
[c] School of Community and Regional Planning, University of British Columbia, Vancouver, Canada
[d] Department of Geography, UC Santa Barbara, Santa Barbara, CA, USA

ARTICLE INFO

Keywords:
Urban heat island
Urban morphology
Sub-saharan africa

ABSTRACT

Urban heat islands (UHI) are an increasingly urgent concern in rapidly urbanizing regions, yet empirical evidence from Sub-Saharan Africa remains limited. This pilot study examines how urban morphology influences UHI intensity across 388 urban settlements in Ghana, Togo, and Tanzania, adapting conventional approaches to data-poor environments. We integrate MODIS land surface temperature with high-resolution land cover and Africapolis settlement boundaries, introducing an adaptive rural baseline that accounts for elevation and cropland exclusions to isolate urban–rural thermal contrasts. Using class-based and landscape-level metrics, we evaluate the role of land use composition, fragmentation, and settlement form in shaping daytime UHI through ordinary least squares regressions. Similar to studies elsewhere, we show that contiguous urban development intensifies UHI, while fragmented urban fabrics help mitigate heat. However, distinctive patterns also emerge. Peri-urban agricultural cohesion significantly reduces UHI, and irregular settlement shapes, often reflecting ribbon-like development along roads, are associated with stronger UHI effects. These findings diverge from results elsewhere, underscoring the importance of context-specific analysis. Methodologically, the study demonstrates that UHI metrics can be adapted to African cities. The results highlight how preserving peri-urban agriculture and maintaining heterogeneous settlement structures can help reduce heat stress in resource-constrained urban environments.

1. Introduction

Cities across Sub-Saharan Africa are experiencing some of the fastest population growth in the world, often in unplanned and informal ways, with the region's urban population projected to more than double by 2050 (United Nations, 2025). This rapid expansion is occurring alongside major environmental pressures including rising temperatures, increasing frequency of extreme heat events, and limited urban green infrastructure, amplifying vulnerability to climate risks (OECD/SWAC, 2020; UN-Habitat, 2022). The expansion of impervious surfaces and loss of vegetated land cover associated with rapid urbanization have been identified as key drivers of the Urban Heat Island (UHI) effect, in which urban areas experience significantly higher temperatures than surrounding rural zones. However, these dynamics may manifest differently in African cities, where large shares of the urban population reside in informal

* Corresponding author.
E-mail address: sjs96@cornell.edu (S. Schmidt).

https://doi.org/10.1016/j.rsase.2026.102005
Received 29 January 2026; Received in revised form 17 March 2026; Accepted 2 April 2026
Available online 5 April 2026
2352-9385/

settlements and where peri-urban landscapes often remain closely integrated with agricultural land uses.

Calculating the surface UHI effect typically involves comparing the average land surface temperature of urban pixels against nearby rural or peri-urban reference areas, and analyzing how urban morphology, such as impervious surface cover, vegetation loss, and building configuration, contributes to observed heat patterns (Weng et al., 2004). Advances in remote sensing and spatial data have enabled increasingly detailed assessments of these relationships, particularly in cities across North America, Europe, and East Asia. However, granular analyses of African urban spatial structure remain rare (Agyemang et al., 2019), and the relationship between the spatial structure of SSA cities and sustainability indicators, such as the urban heat island effect remains particularly underexplored, especially in comparison to extensive studies conducted in North America, Europe, and Asia (Simwanda et al., 2019). Data limitations, inconsistent urban boundary definitions, and the limited availability of high-resolution spatial datasets have historically constrained large-scale comparative research on urban morphology and environmental outcomes in the region.

To address this gap, our study pursues two objectives. First, drawing on newly available open datasets, we develop and document a workflow that adapts conventional urban morphology analysis to settings with lower-resolution and uneven data quality. Second, we assess whether the associations between spatial patterns and the surface UHI observed in data-rich regions of the global north hold in African cities, whose distinctive characteristics, such as widespread informal settlements, urban and peri-urban agriculture, and largely unregulated expansion, may alter or even invert established findings. In doing so, we contribute to a growing body of research examining whether urban sustainability relationships identified in data-rich contexts can be generalized to rapidly urbanizing regions of the Global South To enable meaningful comparison, our framework replicates prior testing approaches while introducing context-specific adjustments to boundary definitions.

Our results contribute both empirically and methodologically to our understanding of urban heat. First, we identify peri-urban agricultural cohesion as a significant cooling factor in African cities, challenging the common view of urban agriculture as marginal. We also find that increased polycentricity may exacerbate the urban heat island effect, underscoring the context-dependent nature of UHI dynamics. Methodologically, the study demonstrates how conventional landscape metrics and UHI definitions can be adapted to data-scarce African settings, particularly through an adaptive rural baseline and the use of class-specific metrics that better capture urban–rural thermal contrasts. These findings highlight the importance of incorporating locally specific spatial and land-use dynamics when evaluating climate mitigation strategies in rapidly urbanizing regions.

The remainder of this paper is organized as follows. We first examine the specific context of urban sub-Saharan Africa, noting unique characteristics and features that may reveal relationships with surface UHI. Section 3 details the data and methodology, including our innovative adaptive radial search approach to operationalizing UHI, the development of both class-based and landscape metrics as well as preliminary scatterplots to begin to explore some of the relationships between variables. Section 4 presents the regression results of both our naïve and multivariate models in which we model the effect of shape and landscape metric on the UHI effect while controlling for a number of climatic variables. Section 5 presents the conclusion and discusses some of the contributions of the research.

2. African context

The relationship between surface UHI and spatial patterns is complex. On the one hand, studies have suggested that a high-density and compact urban development is positively correlated with high urban temperatures (Debbage and Shepherd, 2015; Schwarz and Manceur, 2015), as heat accumulation can be exacerbated and amplified in densely populated urban areas. Concentrated built-up areas absorb and hold heat, and tall buildings can prevent fresh air from circulating and reducing temperatures (Nugroho et al., 2022; Huang et al., 2025). Other research has found, however, that sprawling configurations, with low-density and fragmented urban development, may also exacerbate UHI intensity (Ewing and Rong, 2008; Shreevastava et al., 2019; Stone et al., 2010; Stone and Rodgers, 2001). This is because such cities have larger areas of impervious surfaces and higher per capita heat emission. Specific urban spatial patterns can also exacerbate or mitigate the UHI effect. For example, Li and Schmidt (2024) find that urban green spaces such as parks do mitigate urban heat, but more dispersed and fragmented patterns of green spaces are more effective in reducing the UHI effect compared with more aggregated and contiguous green spaces. In part, this is because multiple smaller green spaces are able to more effectively reduce and break up contiguous urban areas.

However, African cities face a distinct set of challenges that differentiate their urban development trajectories from those of cities in the Global North (Kamana et al., 2024; Cobbinah et al., 2015). These include: (a) rapid urbanization, often through informal and unplanned settlements lacking basic infrastructure, secure land tenure, and essential services (Roy et al., 2018; Gulyani et al., 2005); (b) limited state capacity for urban planning, which has led to fragmented development patterns characterized by disorderly expansion, peri-urban sprawl, and discontinuous built environments (Korah et al., 2019); and (c) heightened environmental vulnerability, including frequent flooding, heat stress, and air pollution, often coupled with limited adaptive capacity (Cobbinah and Finn, 2023). These contextual factors, and the unique built environments they produce, have important implications for the urban heat island (UHI) effect.

Additionally, distinct land use patterns, such as the prevalence of urban agriculture, may introduce local cooling effects in certain areas. The relationship between urban morphology and UHI is further complicated by regional context. For instance, in hot and arid climates with naturally sparse vegetation, the introduction of trees and vegetation in urban areas may produce an inverse effect, creating localized cooling rather than exacerbating heat accumulation. Rapid and unplanned urban growth, particularly in the peri-urban areas of rapidly developing regions of African cities also introduces measurement challenges. The blurred boundaries between rural and urban areas in many SSA contexts make it difficult to accurately delineate urban extents, potentially leading to classification errors in remote sensing–based UHI measurement.

This project addresses two core challenges: first, how to effectively measure the urban heat island effect in SSA cities given their unique characteristics and distinctive forms of urbanization; and second, how to explain variation in UHI as a function of specific built environment characteristics, including land cover aggregation, fragmentation, and spatial configuration. Next, we introduce our data and methods.

3. Methods and data preparation

This study draws upon a range of environmental and geospatial datasets to examine urban thermal patterns across selected African cities. We conducted a pilot analysis in three Sub-Saharan African countries, Ghana, Togo, and Tanzania; comprising 388 urban settlements (see Fig. 1 below). Settlements are delineated from Africapolis urban agglomerations (population >10,000), which provide continent-wide, consistently mapped settlement polygons. Temporal coverage centers on the year 2019 for baseline analysis, with 2023 and 2024 used for post-COVID validation and robustness checks.

3.1. *Quantifying the UHI effect*

To calculate the Urban Heat Island (UHI) effect, we obtained day (~13:30) and night (~01:30) Land surface temperatures (LST) derived from MODIS satellite imagery (MYD11A2.061 Aqua Land Surface Temperature and Emissivity 8-Day Global 1 km) (Han et al., 2022; Li and Schmidt, 2024) and averaged two-month snapshots from January to February, corresponding to the relatively dry, warm and clear-sky period in our study areas, to reduce cloud and retrieval noise (Sismanidis et al., 2022; Voogt and Oke, 2003). Although limiting the generalizability of the analysis across space and time, this will make the impact of the UHI easier to detect. Product accuracy is approximately 1 K for most non-arid regions, with known challenges in very arid settings; we therefore controlled for aridity and local climate. Following conventional practice in previous works (Schwarz et al., 2011; Chen et al., 2006), we define the surface urban heat island (UHI) effect as the temperature difference between average land surface temperature (LST) in the urbanized area and an appropriately defined rural domain.

$$UHI = T_{U_{mean}} - T_{R_{mean}}$$

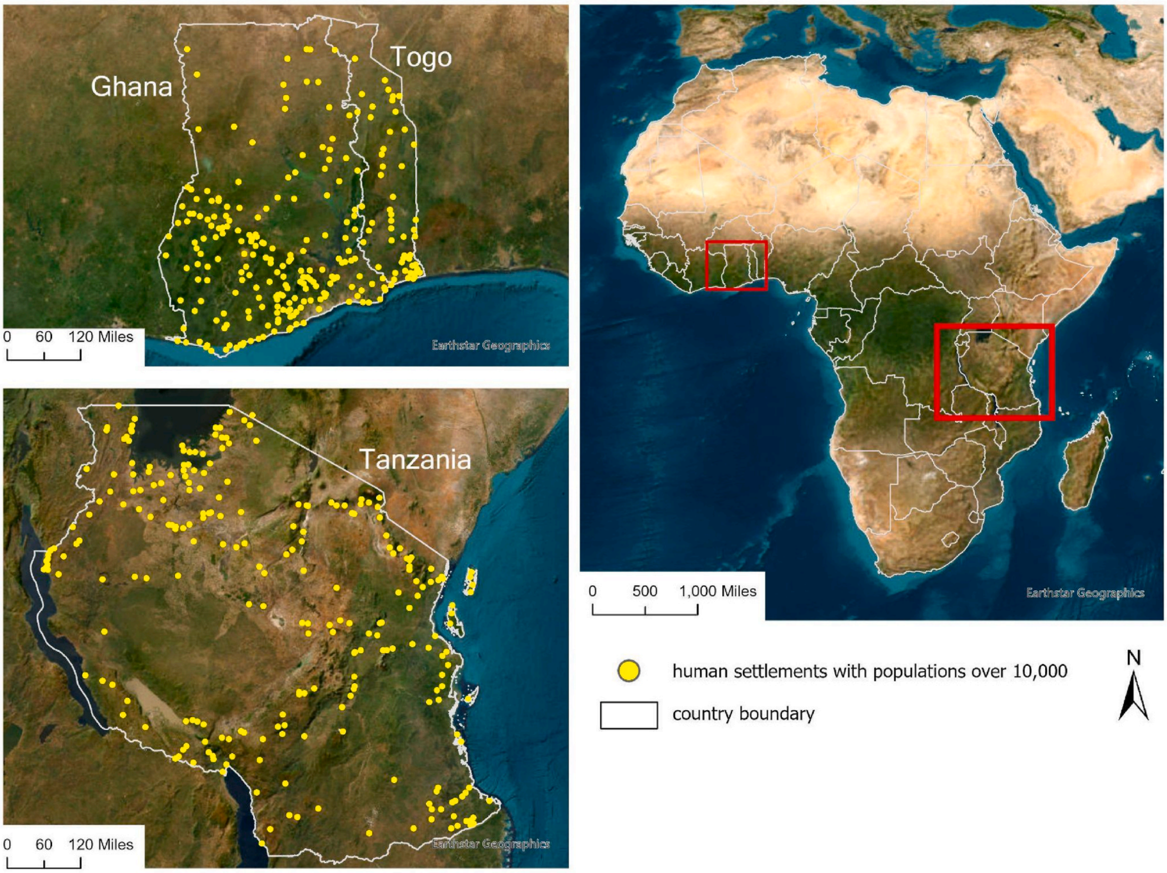

Fig. 1. Study area; 388 urban settlements with populations over 10,000 in three countries (Ghana, Togo, and Tanzania).

This requires both the delineation of discrete urban and rural areas and the computation of mean LST for each. We defined the urbanized area based on the settlement-specific boundary with land-cover filtering. The delineation of urban cores is based on the Copernicus Land Monitoring Service's (CLMS) Land Cover 2019 dataset (100 m). All 100 m cells labeled as built-up (class 50) inside the agglomeration are retained as the urban core for UHI measurement. Fig. 2 below compares the Africapolis settlement boundary, which delineates the broader spatial footprint of human activity, with the urban core extracted from Copernicus land-cover data and used for surface urban heat island (UHI) estimation. The Africapolis boundary captures the full extent of settlement-related land uses, including residential and agricultural among others, and is therefore employed for calculating morphology-related indicators such as land-cover composition, land-use mix, and polycentricity. In contrast, UHI intensity is measured within the more spatially constrained urban core, which isolates contiguous built-up surfaces most directly associated with surface thermal modification. This dual-boundary approach reflects the absence of consistent municipal definitions across African cities and allows morphology metrics to represent settlement-scale human activity while avoiding thermal dilution from sparsely developed land when estimating UHI. Because LST (1 km) is coarser than land cover (100 m), we compute exact area-weighted means for the urban mask so that fractional overlaps contribute proportionally to T(Umean). More generally, all raster-to-polygon summaries in the study use area-weighted extraction to ensure that partially overlapping cells contribute proportionally. This avoids bias from mixed pixels common in small African settlements, mitigates edge effects and ensures accurate representation for irregular urban forms.

3.1.1. Adaptive rural domain

Prior studies often define the rural baseline as non-artificial land cover within a fixed hinterland or administrative ring (Debbage and Shepherd, 2015; Liu et al., 2021). In the African context, however, inconsistently defined administrative boundaries, extensive scattered peri-urban development, and wide variation in settlement sizes can lead to substantial measurement inconsistencies. To address these challenges, we adapt the method proposed by Liu et al. (2021), which generates a series of buffer zones around each urban polygon using an adaptive search approach. Fig. 2 illustrates the adaptive search method used to define an appropriate rural reference area for surface urban heat island (UHI) calculation. For each settlement, we first delineate the urban core from Copernicus built-up land cover within the Africapolis agglomeration boundary. We then generate a series of candidate rural rings around the urban core sealed to the settlement size, indexed from ring 1 to ring 20 in equal ratio increments (see Fig. 3 below). For each candidate ring, we remove all cells classified as urban, water, or cropland and apply an elevation filter using 30 m SRTM data, retaining only pixels within ±100 m of the urban core's mean elevation to mitigate the temperature bias introduced by elevation (Debbage and Shepherd, 2015). Cropland, though later used to calculate related morphological indicators, was excluded because its thermal behavior is not uniform in direction. Empirical evidence shows that croplands can either cool or warm the land surface, depending on irrigation, evapotranspiration, and agricultural practice rather than land-cover class alone (Chen et al., 2024). To avoid biasing the rural reference temperature in either direction, we exclude cropland from baseline construction and instead define the rural reference using non-urban, non-cropland surfaces subject to the same elevation and land-cover filters described above. For each filtered ring, we compute a ring-specific rural mean temperature using area-weighted extraction of the native 1 km MODIS LST raster dataset. Across the full settlement sample, we then compare ring-specific rural means and define "stability" as the smallest ring at which the mean rural temperature no longer differs significantly from the next ring, and the subsequent changes remain negligible. In our sample, both the mean and median daytime UHI estimates show a decreasing trend, but this decline becomes progressively weaker and visually approaches a plateau around ring 8. In the absence of a formal statistical stopping rule, we interpret this pattern as descriptive evidence that the rural baseline becomes relatively insensitive to further ring expansion beyond this point. Ring 8 was therefore selected as a

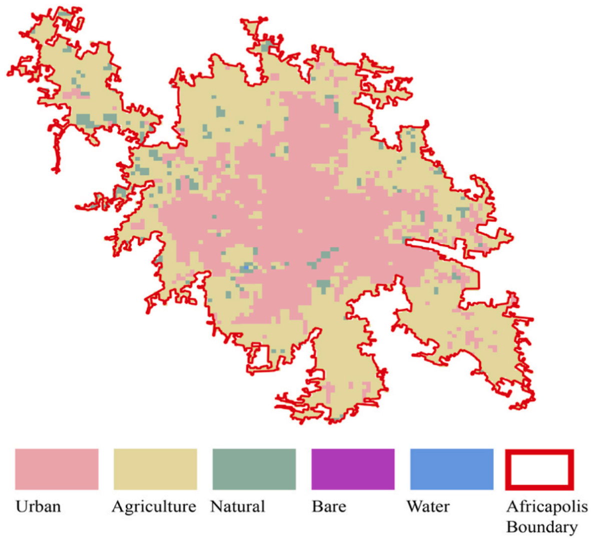

Fig. 2. Dual spatial definitions used for morphology and UHI measurement.

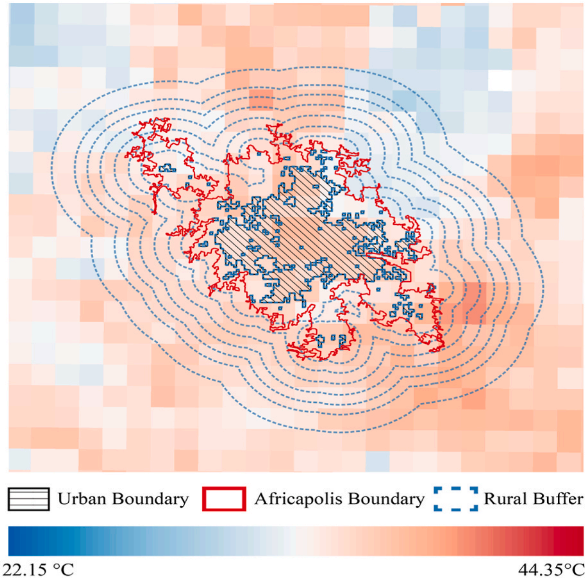

Fig. 3. Adaptive buffer delineation for rural reference temperature estimation.

practical and consistent reference size for cross-settlement comparison. The iterative buffer expansion allows the rural reference to be selected based on spatial context rather than a fixed distance threshold, reducing sensitivity to settlement size, morphology, and surrounding land-use heterogeneity.

3.2. Calculating the urban metrics

We quantify urban spatial patterns using the same family of “traditional” landscape metrics and a morphological polycentricity index as previous studies by Debbage and Shepherd (2015), Liu et al. (2021), Stone et al. (2010), Li and Schmidt (2024), and Li et al. (2026), computed with the *landscapemetrics* implementation of classic FRAGSTATS measures (McGarigal and Marks, 1995). We created metrics for both the urban footprint and the different land cover types in the more generally defined urban boundary by Africapolis, so that class-specific structure and whole landscape mixing can be examined side-by-side.

Table 1
The equation and definition of landscape metrics and polycentricity index following the classic work by McGarigal and Marks (1995).

Metric	Equation and definition	
Percentage of like adjacencies (PLADJ)	$PLADJ_i = \frac{g_{ii}}{\sum_{k=1}^{m} g_{ik}}*100$	g_{ii} = number of adjacent pairs of pixels in land-use class i. g_{ik} = number of adjacent pairs of pixels between land-use class *i* and *k*. m = number of land-use classes in the landscape.
Patch density (PD)	$PD_i = \frac{n_i}{a_i}*10000*100$	n_i = number of patches in class *i*. a_i = total area of class *i*.
Contagion index (CONTAG)	$CONTAG = \left\{1 + \frac{1}{2\,ln(m)}\left[\left(\sum_{i=1}^{m}\sum_{k=1}^{m} p_i \frac{g_{ii}}{\sum_{k=1}^{m} g_{ik}}\right) - ln\,p_i \frac{g_{ii}}{\sum_{k=1}^{m} g_{ik}}\right]\right\}*100$ g_{ik} = number of adjacent pairs of pixels between class *i* and *k*. All pairs of pixels in the adjacency matrix are double counted.	
Area-weighted mean shape index (AWMSI)	$AWMSI_i = \sum_{j=1}^{n}\left[\left(\frac{0.25p_{ij}}{\sqrt{a_{ij}}}\right)\left(\frac{a_{ij}}{\sum_{j=1}^{n} a_{ij}}\right)\right]$	P_{ij} = perimeter of patch *j* in class *i*. a_{ij} = area of patch *ij*. n = total number of patches in class *i*.
Landscape Shape Index (LSI)	$LSI = \frac{0.25*E}{\sqrt{A}}$	E = total length of all patch edges A = total area.
Polycentricity index (POLY)	*Step*1: $P_i(n) = 1 - \frac{\sigma_n}{\sigma_{max}}, (n = 2, 3, 4)$ Step 1: $P_i(n)$ = degree of polycentricity for region *i* incorporating the top n centers. σ_n = standard deviation of population for the top n centers. σ_{max} = the maximum standard deviation of population of an absolute monocentric two-center scenario, namely one center with zero population and another with the maximum population in the region. Step 2: $POLY_i$ = the average degree of polycentricity considering $P_i(2), P_i(3), and\ P_i(4)$.	*Step*2: $POLY_i = \frac{P_i(2) + P_i(3) + P_i(4)}{3}$

3.2.1. *Class-based metrics*

To calculate landscape metrics originally developed by McGarigal and Marks (1995), the 100-m resolution Copernicus land service raster was utilized. This data was clipped to the regions of interest and reclassified into three analysis groups with distinct thermal behavior and spatial distribution: Urban (artificial surfaces), Agriculture, Rural (forest and semi-natural); water is kept separate for masking. The equation and definition for each metric can be found in Table 1. To capture within-class aggregation and fragmentation, we compute for each land cover class *i*.

The percentage of like adjacencies (PLADJ), which quantifies the degree of spatial aggregation of a specific landcover by measuring the frequency of adjacent pixels between the focus class and other classes. Increasing PLADJ values indicate a more aggregated pattern

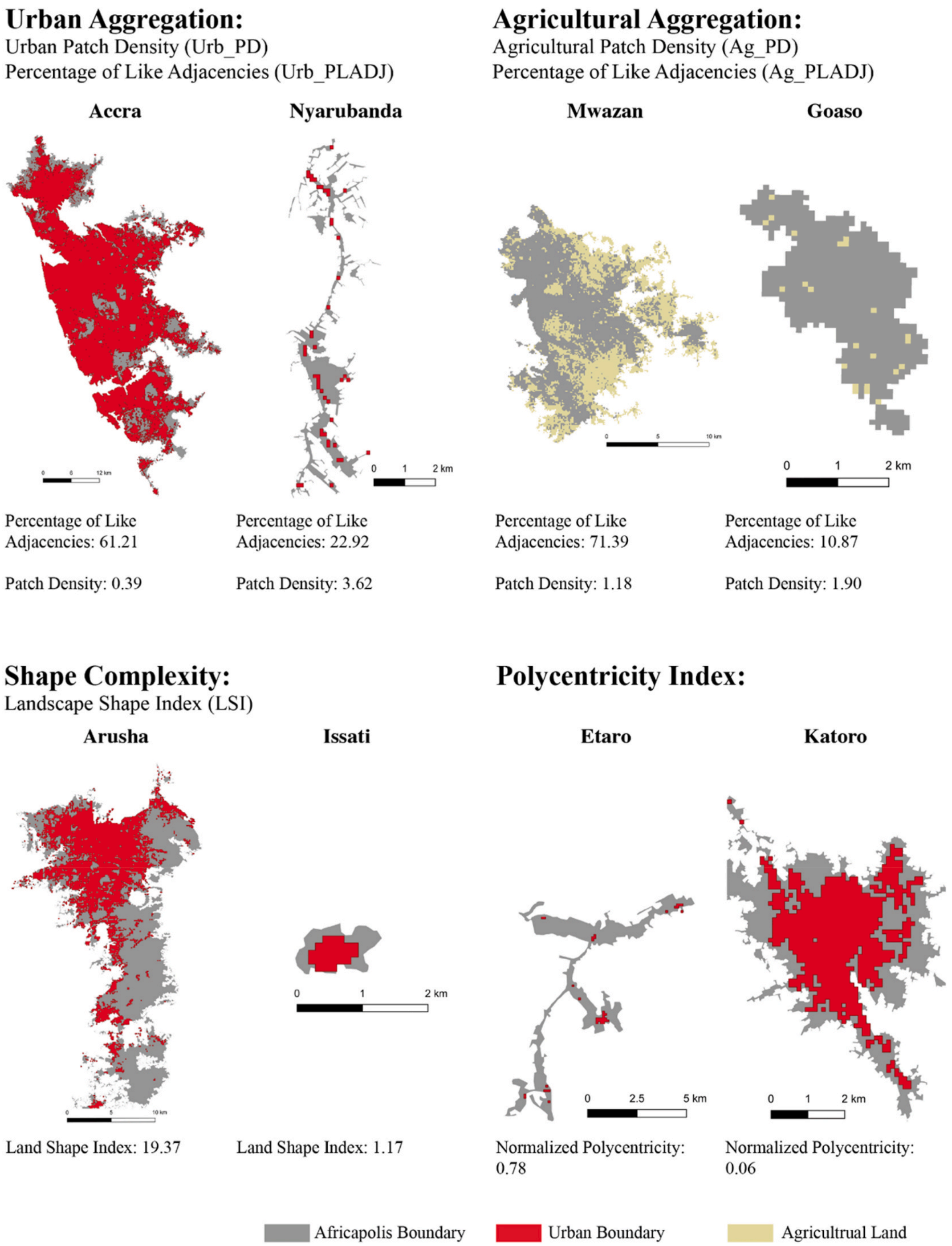

Fig. 4. Spatial characteristics and interpretation of urban morphology indicators.

for pixels of the focus class. Previous research has shown that aggregation of either urbanized areas or green spaces across a metropolitan area can have a significant effect on temperature (Li and Schmidt, 2024).

Patch density (PD) evaluates the degree of fragmentation of urban footprint by measuring the number of urban patches per region. PD is considered the opposite of PLADJ, as higher PD values indicate a patchier and more fragmented landscape pattern. Similar to relevant studies in Germany, the United States, and China (Debbage and Shepherd, 2015; Liu et al., 2021; Li and Schmidt, 2024), we expect a more aggregated urban fabric will intensify the UHI, whereas more dispersed green spaces will have a cooling effect.

The area-weighted mean shape index (AWMSI) quantifies the degree of patch irregularity, giving greater weight to larger patches. It reflects how irregular or compact the dominant land-cover patches are within a landscape, describing the overall shape complexity of the area, but emphasizing the influence of large features like major urban cores or agricultural zones. Li and Schmidt (2024) found that in Germany, more irregular shapes are correlated with higher UHI.

3.2.2. Landscape-level mixing and shape

The metrics in the landscape-level set summarize the joint urban fabric formed by the above-mentioned four classes. The contagion index (CONTAG) quantifies the degree of mixed land use at the landscape level by measuring the probability of adjacent pixels belonging to the same landcover. Higher value means a more homogeneous landscape, and is associated with warmer cities in previous studies (Li and Schmidt, 2024).

The Landscape Shape Index (LSI) quantifies the complexity of the shape of a landscape or its patches relative to a simple, compact form (typically a square). It measures how irregular or fragmented the boundaries of all patches in a landscape are, with higher values indicating greater shape complexity or fragmentation.

3.2.3. Macro-structure

The polycentricity index quantifies the extent to which inhabitants are evenly distributed throughout a city region, using a modified morphological polycentricity approach based on Zhang and Derudder (2019) and Li and Schmidt (2024). The calculation of the polycentricity index involves two steps. In the first step, we determine the degree of polycentricity by benchmarking the standard deviation (SD) of municipality populations against the SD of a hypothetical region characterized by the highest degree of monocentricity, while considering a fixed number of centers. In the second step, we compute the final polycentricity index for each region by averaging the polycentricity indices derived from the top two, three, and four centers. A higher value implies a greater degree of polycentricity.

Fig. 4 below illustrates representative spatial configurations associated with the main morphological indicators used in the analysis, illustrating how different dimensions of settlement structure are operationalized and interpreted. Urban Patch Density (Urb_PD) measures the number of discrete urban patches per unit area, with higher values indicating more fragmented and discontinuous urban fabric. Percentage of Like Adjacencies (Urb_PLADJ) captures the degree of spatial contiguity among urban pixels, with higher values reflecting more compact and internally connected urban areas. In combination, high patch density with low like adjacencies characterizes fragmented and dispersed development, whereas low patch density with high percentage of like adjacencies indicates consolidated urban cores. Empirically, more contiguous urban aggregation is associated with stronger UHI intensity, while fragmentation tends to weaken surface heat accumulation. Agricultural Patch Density (Ag_PD) reflects the fragmentation of agricultural land within the settlement region, with higher values indicating dispersed or interspersed agricultural patches. Agricultural PLADJ (Ag_PLADJ) measures the spatial cohesion of agricultural land. The Landscape Shape Index quantifies the geometric complexity of urban boundaries relative to a compact reference shape. Higher LSI values indicate more irregular, elongated, or perforated urban forms, often reflecting leapfrog or corridor-based development. The polycentricity index captures the degree to which population or built-up intensity is distributed across multiple centers within the settlement boundary. Higher values indicate more evenly distributed subcenters, while lower values reflect monocentric concentration.

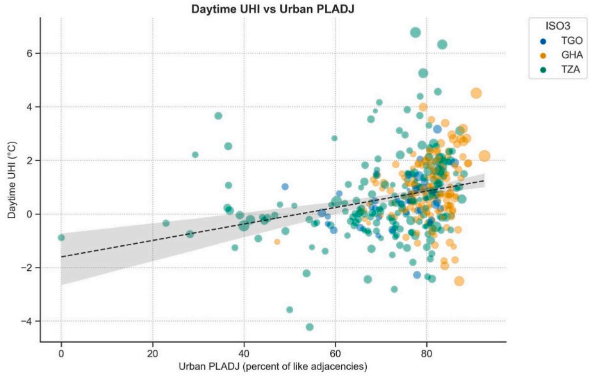

Fig. 5. The relationship between urban percentage of like adjacency on x-axis (PLADJ) and daytime Urban heat island effect on y-axis (UHI_day).

3.3. The relationship between landscape metrics and UHI

Before conducting the regression analysis, we first visualize the impacts of urban morphology on temperature to gain some clues on their relationship. Figs. 5 and 6 below illustrate some of the relationships between our shape metrics and the daytime UHI effect (data points are color coded by country and sized according to urban population). The results suggest a positive and statistically significant association between the PLADJ of urban patches and the UHI effect, indicating that a higher level of aggregation and contiguity in urban patches contributes to increased urban heat intensity. This reflects how more contiguous urban areas trap heat**,** reduce surface ventilation, and limit vegetated cooling. Points are likely clustered more tightly at higher PLADJ values in large metropolitan cores, suggesting the strongest heat intensities occur where the urban landscape is most connected.

Higher agricultural adjacency, more continuous farmland or vegetation cover is associated with lower surface temperature and weaker UHI effects. The visual pattern likely shows the coolest conditions where agriculture forms large, cohesive zones, emphasizing the **c**ooling and heat-buffering role of urban and peri-agricultural landscapes.

In addition to scatterplots, another useful approach is to visualize the UHI gradient, a method originally developed to model density or land price gradients, which illustrates how UHI intensity changes from the urban core to peri-urban areas. Fig. 7 below presents six UHI gradient plots. Within each plot, urban settlements are categorized into two groups–above (red curve) or below (blue curve) the average value of a given landscape metric–to highlight differences in gradients associated with urban morphology. The six metrics include urban patch density, urban patch adjacency, rural patch density, agricultural patch adjacency, landscape shape index, and polycentricity.

In each plot, the x-axis represents the distance to the urban center, and the y-axis shows the normalized UHI intensity, calculated as the difference between each pixel's LST value and its corresponding urban settlement's rural area average temperature (LST_pixel - Rural_Average_LST). For each urban settlement, the urban center is defined as the pixel with the highest population density within the urbanized area, derived from the LandScan 1 km global population grid dataset. LandScan is one of the most accurate and widely-used global population distribution datasets and represents ambient (24-h average) population, developed by Oak Ridge National Laboratory (Lebakula et al., 2025). Euclidean distance is used to define the distance from each pixel to the urban center. For each urban settlement, we first estimated a UHI gradient curve using locally weighted regression (LOWESS) with a neighborhood bandwidth of 0.05, meaning that each local regression uses the nearest 5% of pixels for estimation, and a tricube distance weighting kernel that assigns higher weight to pixels closer to the evaluation point. We then assigned each settlement UHI curve to the above or below group according to the settlement's metric value. Finally, the distribution of UHI intensity was summarized at 0.5 km distance intervals using boxplots, and the group medians across distance bins are connected to illustrate the overall UHI gradient from the urban core toward the periphery for 388 urban settlements. As robustness checks, we also tested neighborhood bandwidths of 0.10 and 0.15, as well as a Gaussian kernel function. These checks do not alter the overall conclusion drawn from these figures.

Comparing the red and blue curves shows that urban patch density, urban patch adjacency, and agricultural patch adjacency have the most pronounced effects on UHI. For urban patch density, the above-average curve lies below the below-average curve, indicating that more fragmented urban areas tend to exhibit lower UHI effects than more aggregated areas, particularly near the urban core where the gap widens. Urban patch adjacency shows a similar trend, with higher adjacency (more aggregated patches) corresponding to higher temperatures compared to more fragmented areas. For agricultural patch adjacency, higher adjacency also leads to higher temperatures near the urban core. In contrast, the curves for rural patch density, landscape shape index, and polycentricity are close together, suggesting weaker or unclear relationships.

It is important to note that UHI is influenced by multiple confounding factors; these visualizations are descriptive rather than causal. We next present naïve regression models (Table 2), followed by a multivariate OLS regression controlling for population, weather, and climate variables (Table 3).

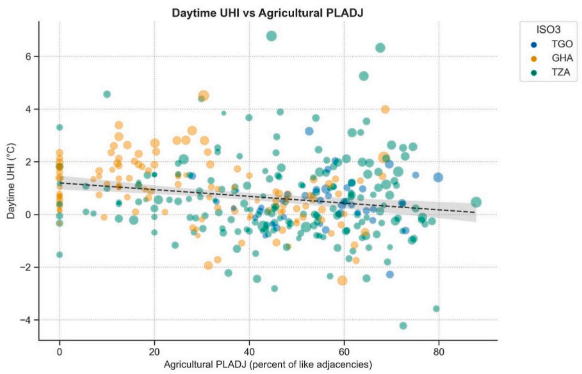

Fig. 6. The relationship between agricultural percentage of like adjacency on x-axis (PLADJ) and daytime Urban heat island effect on y-axis (UHI_day).

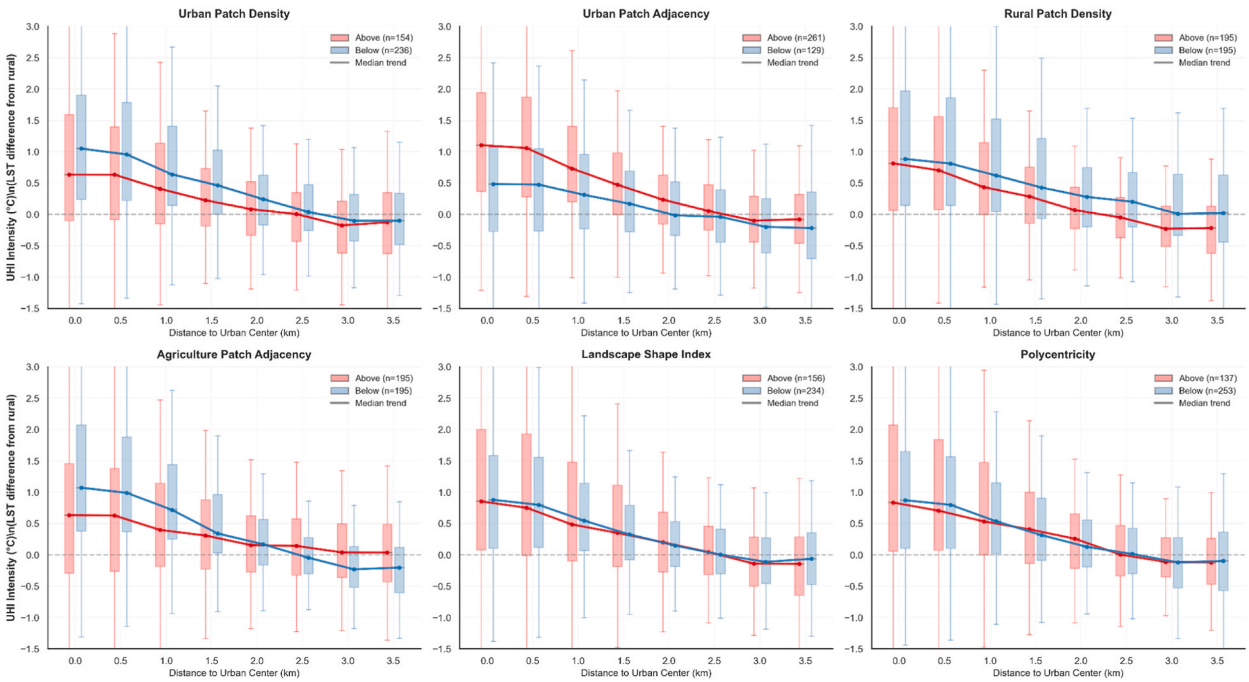

Fig. 7. Urban heat island gradients (LOWESS smoothed) and boxplots for urban settlements grouped by whether a given landscape metric is above (red) or below (blue) the average (group sizes shown in legend).

Table 2
Independent and dependent summary statistics (N = 388).

Variable Name	Mean	Std	Median	Min	Max
Urban heat island	0.493	1.31	0.183	−4.223	6.773
Urban percentage of like adjacencies	69.120	17.168	76.786	29.310	90.829
Urban patch density	1.177	0.834	0.893	0.150	4.478
Rural percentage of like adjacencies	40.219	16.211	39.000	0.187	87.103
Rural patch density	3.874	2.173	3.416	0.124	10.174
Agriculture percentage of like adjacencies	42.690	20.931	47.664	0.000	79.820
Agriculture patch density	2.658	1.610	2.658	0.060	8.801
Landscape contagion	38.810	12.221	41.174	9.317	80.575
Polycentricity index	0.212	0.156	0.153	0.065	0.735
Area weighted mean shape index	2.942	1.482	2.547	1.13	11.493
Landscape Shape Index	4.422	2.379	3.583	1.545	19.373
Aridity Index	33.028	7.091	31.610	17.277	61.922
Wind speed	0.974	0.813	0.875	0.113	5.394
Population density	4054.31	1906.404	3474.04	67.018	15705.9

Table 3
Naive OLS Regression Model Results (n = 388). Each landscape metric is tested independently, along with control variables.

Variable of Interest	Coefficient	Std. Error	P-Value	Significance	R Squared
Urban percentage of like adjacencies	0.0355	0.012	0.0024	***	0.2326
Urban patch density (log)	−0.3362	0.106	0.0015	***	0.2296
Rural percentage of like adjacencies	0.0028	0.004	0.5277		0.2084
Rural patch density (log)	0.3694	0.085	0.0000	***	0.2403
Agriculture percentage of like adjacencies	−0.0124	0.004	0.0010	***	0.2318
Agriculture patch density (log)	0.0260	0.094	0.7820		0.2077
Landscape contagion	−0.0024	0.006	0.6821		0.2079
Area-weighted mean shape index (log)	0.2496	0.132	0.0587	*	0.2113
Landscape Shape Index (log)	−1.0094	0.275	0.0002	***	0.2362
Polycentricity index	0.6770	0.379	0.0090	*	0.2113

Standard errors are reported (****p* < .01, ***p* < .05, **p* < .1).
Note: (1) Each landscape metric is tested independently along with control variables. (2) control variables include aridity index, wind speed, and country dummy variables.

4. Regression analysis

The unit of statistical inference in the regression analysis is the settlement (N = 388), where the dependent variable is the settlement-level UHI estimate and predictors are settlement-level morphology and control variables. Pixel-level LST values are used only in preprocessing and pilot studies to construct area-weighted urban and rural means, and descriptive UHI gradients as in Fig. 6. Accordingly, the p-values reported in Tables 3 and 4 do not rely on treating pixels as independent observations. Spatial autocorrelation at the pixel level may affect the smoothness of the descriptive gradient curves, but it does not determine the inferential statistics reported for the city-level regressions. Prior to modeling, variables were transformed and scaled to meet statistical assumptions. Non-linear relationships were addressed through log-transformations where appropriate. In cases where UHI intensity values included negative values (i.e., rural areas warmer than urban), a constant was added to ensure all values were positive before applying logarithmic transformations. All independent variables were standardized where necessary to allow for meaningful coefficient comparison across units.

In order to control for a number of climate and environmental factors (ie wind speed, precipitation, and temperature), we utilized 9 km resolution ERA5-Land climate data (2019, 2023, 2024) which were converted from GRIB to GeoTIFF format. ERA-5 Land is a widely used land-surface reanalysis product for representing regional background climate conditions rather than intra-urban micro-climatic variation (Muñoz-Sabater et al., 2021). Consistent with all other raster-to-polygon summaries in the study, settlement-level values were extracted using area-weighted averaging, so that each intersecting raster cell contributes proportionally to its overlap with the settlement polygon. We also included the following variables: an Aridity Index, derived from the ratio of precipitation to temperature using the De Martonne formula: I_arid = P/(T + 10), where P is mean precipitation and T is mean temperature. Drier conditions reduce evaporative cooling and tend to amplify UHI effects. Wind speed (ln_ws) is taken from ERA5-Land monthly means. Stronger winds enhance heat dissipation and reduce UHI intensity. Settlement Size considers the log of Copernicus-built artificial surfaces, the log of Africapolis agglomeration area, and the log of settlement population. Combined, they control the intensity of human activity within urban settlements, which contributes to the thermal production and retention in urban areas. Country fixed effects (country_dummies) are also included to absorb unobserved heterogeneity in climate, governance, and regional data quality across Ghana, Togo, and Tanzania.

To assess multicollinearity, we calculated variance inflation factors (VIFs) for both the control variables and candidate predictors. Collinearity was concentrated among variables describing urban aggregation and fragmentation, spatial configuration, and background climate. In response, we removed and aggregated several highly redundant variables, including urban area, elongation, and sprawl. Some theoretically distinct variables with elevated VIFs are retained to capture analytically important but partly overlapping dimensions of settlement morphology or environmental context. For example, Urban PLADJ (VIF = 21.3) and urban patch density are strongly negatively correlated in many settlements sharing the monocentric urban aggregation. Likewise, the landscape contagion index (VIF = 14.2) overlaps with class-specific aggregation measures as all reflect the landcover configuration. These coefficients are therefore interpreted cautiously given their internal correlation, rather than as perfectly independent marginal effects.

To test the baseline association between individual spatial metrics and the surface urban heat island (UHI) effect, we constructed a series of naive ordinary least squares (OLS) models. Each model regresses day-time UHI on a single independent metric of interest, controlled by a consistent set of climatic and demographic covariates. The generic specification of the model is as follows:

$$UHI_i = c + \beta_1 X_i + \mu Z_i + \epsilon_i$$

Where X_i is one spatial metric for settlement i; Z_i is a vector of control variables, and ϵ_i is the error term. Descriptive summary statistics for all variables are provided in Table 2 below.

Table 4
Multi-Variable Regression Results (n = 388, r2 = 0.291, adj. R2 = 0.261).

Variable	Coef.	Std Error	VIF	P-value	Significance
constant	−3.6521	1.423		0.010	**
Urban percentage of like adjacencies	0.0203	0.009	21.3	0.030	**
Urban patch density (log)	−0.3684	0.113	1.8	0.001	***
Rural percentage of like adjacencies	−0.0029	0.007	10.2	0.667	
Rural patch density (log)	0.2053	0.101	5.0	0.041	**
Agriculture percentage of like adjacencies	−0.0143	0.005	9.2	0.004	***
Agriculture patch density (log)	0.0447	0.128	3.0	0.728	
Landscape contagion	0.0009	0.01	14.2	0.930	
Area weighted mean shape index (log)	0.1445	0.124	12.1	0.245	
Landscape Shape Index (log)	0.5719	0.264	27.7	0.030	**
Polycentricity index	0.9825	0.447	4.0	0.028	**
Aridity index	0.032	0.012	26.1	0.010	**
Wind speed (log)	0.0117	0.094	1.7	0.901	
TGO (dummy variable)	0.6423	0.284	1.9	0.023	**
TZA (dummy variable)	0.6629	0.249	5.0	0.008	***

Standard errors are reported (***p < .01, **p < .05, *p < .1*).
Note: all listed variables are included in a single regression model. Coefficient estimates with 95% confidence intervals are shown in Appendix Table A1 and Figure A1.

Initially, separate models were specified for daytime and nighttime LST to account for diurnal variation in UHI effects, but the nighttime model was excluded due to its weak relationship with landscape features after controlling for population and size. This may limit the generalizability of the analysis, but nighttime dissipation effects may be governed more by energy use than spatial patterns. Table 3 reports the results of these naive OLS regressions, showing coefficients, significance, and model fit (R^2) for each metric tested independently, while Table 4 are the multi-variable regression results.

Residual Moran's I diagnostics indicate modest positive spatial autocorrelation in the OLS residuals. As a robustness check, we therefore estimated spatial error models under multiple spatial weights matrices. The spatial error parameter was significant across all specifications, and residual spatial autocorrelation was no longer detected in the SEM innovations (Appendix B). The models demonstrate that several, though not all, landscape metrics examined in prior studies have significant effects on daytime UHI. The results indicate that urban fragmentation can help mitigate heat, consistent with findings by Debbage and Shepherd (2015) and Li and Schmidt (2024). Specifically, greater spatial aggregation of urban patches (Urban percentage of like adjacencies) is linked to stronger daytime UHI. The effect is positive and significant in both models, suggesting that greater spatial clustering of urban patches is associated with higher daytime UHI intensity. The effect size is smaller in the multivariable model, indicating that part of the naïve effect is shared with other correlated metrics.

Similarly, higher urban patch fragmentation (an increase in urban patch density) is associated with lower UHI, and is significant in both models, implying that more fragmented or numerous urban patches are linked to lower UHI values, possibly reflecting ventilation effects or heterogeneity in built-up structure. This pattern reflects the basic mechanism of UHI formation: contiguous artificial surfaces concentrate and retain heat, whereas a more fragmented urban fabric allows for ventilation and interaction with cooler non-urban land covers.

In both models, rural patch adjacency remains insignificant, while rural patch density is positive and significant, although the coefficient declines (from 0.369 to 0.205) when controlling for other land-use types. This suggests that breaking up contiguous natural cover reduces the peri-urban cooling ability. In many African settlements, large formal parks are rare and zoning or green-space regulations are limited. As a result, rural patch aggregation within the settlement boundary may be low and unhelpful in explaining surface temperature differences. By contrast, an increase in the fragmentation of rural land at the urban periphery through unplanned and haphazard development structure limiting its cooling impact.

Excluding cropland from the rural baseline does not imply that agricultural land is thermally irrelevant. In our framework, the exclusion of cropland serves a measurement purpose to prevent agriculture-specific cooling or warming effects from being absorbed into the baseline. The association between peri-urban agricultural landscapes and lower or higher settlement temperatures is interpreted separately here as a possible explanatory process. Agricultural cohesion (Agricultural percentage of like adjacencies) is negatively associated with thermal intensity and significant in both tables, implying that greater contiguity of agricultural land mitigates urban heat. The consistency across models highlights a robust cooling influence of agricultural landscapes. However, this directional expectation should be understood as a likely tendency rather than a universal rule, since the thermal behavior of cropland may vary by season, irrigation regime, crop type, and background climate. By contrast, agricultural patch density is not significant. This likely reflects the widespread presence of peri-urban farming belts across African settlements, which makes patch density relatively uniform and limits its explanatory power. Agricultural cohesion serves as an indirect proxy for the width and continuity of these belts: wider, more cohesive agricultural zones are better able to sustain evapotranspiration and buffer urban heat, resulting in the observed negative coefficient. Unlike croplands in more developed regions, where mechanization, bare-soil intervals, and plasticulture often reduce latent cooling, African agriculture tends to involve smallholder mosaics, scattered trees, mixed cropping, and basic irrigation systems that maintain near-surface moisture. Together, these characteristics explain why agricultural patch aggregation emerges as significant, while agricultural patch density, being more homogeneous across settlements, does not.

The area-weighted mean shape index is only marginally significant in Table 2 and becomes insignificant in Table 3, suggesting its apparent effect is mediated by other land-use factors. The Landscape Shape Index (LSI), however, changes sign—negative and significant in the naïve model, but positive and significant in the multivariable model. This reversal indicates a suppression or collinearity effect, where the inclusion of multiple correlated landscape metrics alters the net relationship between shape complexity and heat intensity. The positive correlation is similar to the findings of Li and Schmidt (2024), who report that shape irregularity is typically associated with stronger UHI effects. A possible explanation is that in many African agglomerations, where density and overall size are limited, irregular or elongated footprints often reflect ribbon-like growth along transport corridors. Likewise, our null result for Landscape contagion (overall landscape homogeneity) suggests that in African contexts, where urban–rural boundaries are blurred and urban cores remain heterogeneous and weakly regulated, a global "mixed land use" index is less informative than class-specific metrics such as patch density and patch adjacency.

These results are broadly consistent with prior studies, demonstrating that more homogeneous urban patches intensify UHI, while rural patches help to mitigate it. Yet, notable differences emerge at the macro scale. Of particular note, the polycentricity index is significant, indicating that increased polycentricity exacerbates the urban heat island effect. This finding contrasts with prior research (Li and Schmidt, 2024), which identified a negative relationship between polycentricity and heat. The divergence suggests that the spatial structure of African cities operates differently: instead of dissipating heat over a broader area, polycentric development in peripheral urban regions often consists of high-density, informal settlements with limited amenities such as tree cover or transit accessibility; factors that might otherwise mitigate urban heat.

5. Discussion

Our study demonstrates that spatial patterns of land use and urban morphology exert measurable and often distinctive influences on the surface urban heat island (UHI) effect in Sub-Saharan African cities. Consistent with findings elsewhere, we find that contiguous urban development intensifies UHI, while fragmented or perforated landscapes provide some degree of cooling. However, several results diverge from patterns observed elsewhere, underscoring the importance of examining UHI in African cities on their own terms rather than through studies from other regions.

This study is subject to several important limitations. First, data resolution constraints may affect measurement precision, particularly given the mismatch between 1 km MODIS land surface temperature data and finer-resolution land cover and settlement boundary datasets, despite the use of area-weighted adjustments. Second, temporal misalignment among datasets introduces potential uncertainty, as land cover (2019), climate variables, settlement boundaries, and validation years (2023–2024) do not perfectly coincide, which may influence estimated associations. Finally, while the multi-country design strengthens internal comparison, the findings are derived from 388 settlements in Ghana, Togo, and Tanzania during a specific study period and may not be fully generalizable to other Sub-Saharan African contexts, different climatic zones, or longer-term urbanization trajectories. These considerations should be taken into account when interpreting the results and extending the conclusions to broader settings.

That said, one of the most policy-relevant findings is the robust cooling effect of urban and peri-urban agriculture. Unlike in many Global North contexts where peri-urban agriculture is declining or highly mechanized, agricultural belts remain extensive and spatially interwoven with settlements in Ghana, Togo, and Tanzania. Our results show that the contiguity of these agricultural zones, and not merely their presence, reduces UHI intensity.

This finding reframes peri-urban agriculture as climate infrastructure. In terms of governance, agricultural land in African cities is often viewed as either marginal or transitional, awaiting conversion to residential or commercial uses. Yet the results suggest that maintaining continuous agricultural belts can buffer urban heat, and suggest a number of policy implications. These include integrating agricultural protection into metropolitan land-use plans not solely for food security but for heat mitigation, avoiding piecemeal encroachment that fragments agricultural belts, and recognizing that informal agricultural areas may provide ecological services comparable to formally designated green spaces. As such, preserving peri-urban agriculture may represent a cost-effective climate adaptation strategy relative to more engineered cooling interventions.

The positive association between landscape shape irregularity and UHI in the multivariate model likely reflects ribbon-like expansion along transport corridors and arterial roads. Such development often produces elongated, discontinuous settlement forms with extensive edge conditions but limited internal green buffering. In the African context, transport-led growth frequently precedes planning and formal infrastructure provision. The thermal implications of corridor urbanization therefore warrant attention. Regional spatial plans could mitigate heat risks by establishing green setbacks along major corridors or designing linear development with integrated vegetated buffers.

Methodologically, the study contributes by demonstrating the feasibility of adapting conventional landscape metrics and UHI definitions to data-scarce African settings. Our adaptive rural baseline, which accounts for local elevation and excludes irrigated croplands, provides a replicable approach for isolating urban–rural thermal contrasts in heterogeneous landscapes. The results also highlight the importance of class-specific metrics: agricultural and rural patch measures yielded stronger associations with UHI than generic landscape homogeneity indicators, reflecting the urban–rural fabric in many African cities.

CRediT authorship contribution statement

Stephan Schmidt: Writing – review & editing, Writing – original draft, Project administration, Investigation, Funding acquisition, Conceptualization. **Yucheng Zhang:** Writing – original draft, Visualization, Methodology, Investigation, Formal analysis, Data curation. **Wenzheng Li:** Methodology, Investigation, Formal analysis. **Houpu Li:** Formal analysis, Data curation.

Ethical statement

The work described has not been published previously except in the form of a preprint, an abstract, a published lecture, academic thesis or registered report.

The article is not under consideration for publication elsewhere.

The article's publication is approved by all authors and tacitly or explicitly by the responsible authorities where the work was carried out.

If accepted, the article will not be published elsewhere in the same form, in English or in any other language, including electronically, without the written consent of the copyright-holder.

Declaration of competing interest

The authors declare that they have no known competing financial interests or personal relationships that could have appeared to influence the work reported in this paper.

Appendix A. Additional regression results reporting

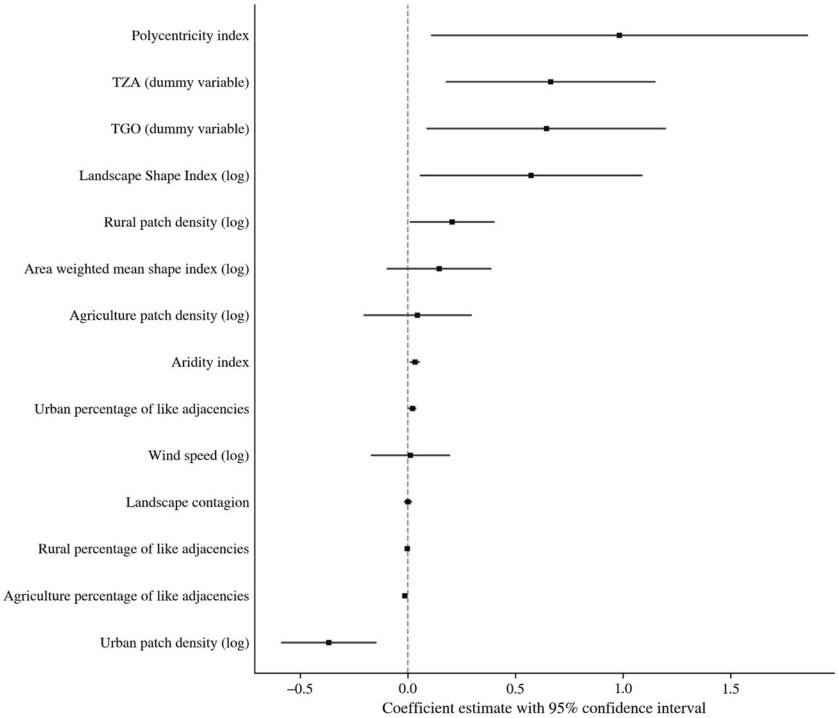

Fig. A1. Coefficient estimates with 95% confidence intervals for the main settlement-level multivariable OLS model. Confidence intervals are based on HC3 robust standard errors.

Table A1
95% confidence intervals for the main settlement-level multivariable OLS model.

Variable	Lower 95 CI	Upper 95 CI
constant	−6.441	−0.863
Urban percentage of like adjacencies	0.002	0.039
Urban patch density (log)	−0.59	−0.147
Rural percentage of like adjacencies	−0.016	0.01
Rural patch density (log)	0.008	0.402
Agriculture percentage of like adjacencies	−0.024	−0.004
Agriculture patch density (log)	−0.207	0.296
Landscape contagion	−0.019	0.02
Area weighted mean shape index (log)	−0.099	0.388
Landscape Shape Index (log)	0.055	1.089
Polycentricity index	0.107	1.858
Aridity index	0.008	0.056
Wind speed (log)	−0.173	0.196
TGO (dummy variable)	0.087	1.198
TZA (dummy variable)	0.176	1.15

Appendix B. Spatial dependence diagnostics and SEM robustness checks

Table B1
Residual Moran's I and SEM robustness diagnostics across alternative spatial weights matrices

Weight specification	Lambda	Lambda p-value	OLS residual Moran's I	OLS residual Moran p-value	SEM innovation Moran's I	SEM innovation Moran p-value
Distance: 200 km	0.5474	0.0000	0.0372	0.0220	−0.0119	0.5220
Distance: 300 km	0.6789	0.0000	0.0275	0.0240	0.0008	0.6260
KNN: 5	0.2552	0.0103	0.0562	0.0340	−0.0105	0.8740
KNN: 8	0.3253	0.0052	0.0479	0.0400	−0.0172	0.5320

To assess whether residual spatial dependence existed in the OLS model, we calculated Moran's I for the OLS residuals under four alternative spatial weights matrices: fixed-distance bands of 200 km and 300 km, and k-nearest-neighbor specifications with k = 5 and k = 8. Across all four weighting methods, Moran's I was positive and statistically significant, but with a relatively small magnitude (0.028 - 0.056), indicating modest residual spatial autocorrelation in the OLS model. As a robustness check, we estimated spatial error models (SEM) using the same regressors as in the main multivariable OLS specification. The spatial error parameter λ was statistically significant. Under all four spatial weights matrices, Moran's I was no longer statistically significant (p = .522 - 0.874), and the estimated statistics were close to zero. This suggests that the SEM effectively absorbed the residual spatial autocorrelation present in the baseline OLS model. We therefore interpret the OLS results as broadly informative but supplement them with SEM robustness checks to confirm that the main findings are not driven by unmodelled spatial error structure. For transparency and comparability with the existing urban heat literature, we retain the OLS model with HC3 robust standard errors as the main specification in the manuscript.

Table B2
Comparison of key coefficients between OLS-HC3 and SEM specifications

Variable	OLS: HC3	Distance: 200 km	Distance: 300 km	KNN: 5	KNN: 8
Urban percentage of like adjacencies	0.0203	0.0135	0.0133	0.0158	0.0155
Urban patch density (log)	−0.3684	−0.3031	−0.3181	−0.2785	−0.2559
Rural percentage of like adjacencies	−0.0029	−0.0027	−0.0034	−0.0020	−0.0004
Rural patch density (log)	0.2053	0.1032	0.1001	0.1485	0.1419
Agriculture percentage of like adjacencies	−0.0143	−0.0069	−0.0078	−0.0098	−0.0085
Agriculture patch density (log)	0.0447	0.0583	0.0304	0.0264	0.0466
Landscape contagion	0.0009	0.0045	0.0024	0.0035	0.0052
Area weighted mean shape index (log)	0.1445	0.1387	0.1328	0.1575	0.1478
Landscape Shape Index (log)	0.5719	0.5921	0.5474	0.5835	0.6217
Polycentricity index	0.9825	0.8591	0.8266	0.8142	0.7653
Aridity index	0.0320	0.0221	0.0293	0.0320	0.0296
Wind speed (log)	0.0117	−0.0631	−0.1274	0.0363	0.0326
TGO (dummy variable)	0.6423	0.5989	0.6202	0.5891	0.5972
TZA (dummy variable)	0.6629	0.5079	0.5442	0.6110	0.5935

Table B2 compares the coefficient estimates from the main OLS-HC3 model with those from four SEM robustness specifications. The comparison shows that coefficient directions are highly stable across models. SEM robustness checks do not overturn the interpretation based on the main multivariate OLS model, but they do attenuate the statistical significance of several marginal OLS associations. The most stable findings lie within urban-related shape matrices, shape index, and aridity, while several rural-structure-related coefficients become modestly weaker.

Data availability

Data will be made available on request.

References

Cobbinah, P.B., Erdiaw-Kwasie, M.O., Amoateng, P., 2015. Africa's urbanisation: implications for sustainable development. Cities 47, 62–72.
Cobbinah, P.B., Finn, B.M., 2023. Planning and climate change in African cities: informal urbanization and 'Just'Urban transformations. J. Plann. Lit. 38 (3), 361–379.
Chen, C., Li, Y., Wang, X., Luo, X., Li, Y., Cheng, Y., Zhu, Z., 2024. Biophysical effects of croplands on land surface temperature. Nat. Commun. 15 (1), 10901.
Chen, X.L., Zhao, H.M., Li, P.X., Yin, Z.Y., 2006. Remote sensing image-based analysis of the relationship between urban heat island and land use/cover changes. Rem. Sens. Environ. 104 (2), 133–146.
Debbage, N., Shepherd, J.M., 2015. The urban heat island effect and city contiguity. Comput. Environ. Urban Syst. 54, 181–194.
Ewing, R., Rong, F., 2008. The impact of urban form on U.S. residential energy use. Hous. Pol. Debat. 19 (1), 1–30.
Gulyani, S., Talukdar, D., Mukami Kariuki, R., 2005. Universal (non) service? Water markets, household demand and the poor in urban Kenya. Urban Stud. 42 (8), 1247–1274.
Han, S., Li, W., Kwan, M.P., Miao, C., Sun, B., 2022. Do polycentric structures reduce surface urban heat island intensity? Appl. Geogr. 146, 102766.
Huang, C., Liu, K., Ma, T., Xue, H., Wang, P., Li, L., 2025. Analysis of the impact mechanisms and driving factors of urban spatial morphology on urban heat islands. Sci. Rep. 15 (1), 18589.
Kamana, A.A., Radoine, H., Nyasulu, C., 2024. Urban challenges and strategies in African cities–a systematic literature review. City Environ. Interact. 21, 100132.
Korah, P.I., Matthews, T., Tomerini, D., 2019. Characterising spatial and temporal patterns of urban evolution in Sub-Saharan Africa: the case of Accra, Ghana. Land Use Policy 87, 104049.
Lebakula, V., Sims, K., Reith, A., Rose, A., McKee, J., Coleman, P., et al., 2025. LandScan global 30 arcsecond annual global gridded population datasets from 2000 to 2022. Sci. Data 12 (1), 495.
Li, W., Schmidt, S., 2024. Can spatial patterns mitigate the urban heat island effect? Evidence from German metropolitan regions. Environ. Plan. B Urban Anal. City Sci. 51 (8), 1948–1964.
Li, W., Schmidt, S., Gu, J., 2026. Regional polycentric spatial patterns and air pollution: an empirical study of German metropolitan regions. Cities 170, 106676.
Liu, H., Huang, B., Zhan, Q., Gao, S., Li, R., Fan, Z., 2021. The influence of urban form on surface urban heat island and its planning implications: evidence from 1288 urban clusters in China. Sustain. Cities Soc. 71, 102987.
McGarigal, K., Marks, B.J., 1995. FRAGSTATS: Spatial Pattern Analysis Program for Quantifying Landscape Structure. PNW-GTR-351. U.S. Department of Agriculture, Forest Service, Pacific Northwest Research Station, Portland, OR.
Muñoz-Sabater, J., Dutra, E., Agustí-Panareda, A., Albergel, C., Arduini, G., Balsamo, G., Boussetta, S., Choulga, M., Harrigan, S., Hersbach, H., Martens, B., Miralles, D.G., Piles, M., Rodríguez-Fernández, N.J., Zsoter, E., Buontempo, C., Thépaut, J.-N., 2021. ERA5-Land: a state-of-the-art global reanalysis dataset for land applications. Earth Syst. Sci. Data 13 (9), 4349–4383. https://doi.org/10.5194/essd-13-4349-2021.

Nugroho, N.Y., Triyadi, S., Wonorahardjo, S., 2022. Effect of high-rise buildings on the surrounding thermal environment. Build. Environ. 207, 108393.
OECD/SWAC, 2020. Africa's Urbanisation Dynamics 2020: Africapolis, Mapping a New Urban Geography.
Roy, M., Shemdoe, R., Hulme, D., Mwageni, N., Gough, A., 2018. Climate change and declining levels of green structures: life in informal settlements of Dar es Salaam, Tanzania. Landsc. Urban Plann. 180, 282–293.
Schwarz, N., Manceur, A.M., 2015. Analyzing the influence of urban forms on surface urban heat islands in Europe. J. Urban Plann. Dev. 141 (3), A4014003.
Schwarz, N., Lautenbach, S., Seppelt, R., 2011. Exploring indicators for quantifying surface urban heat islands of European cities with MODIS land surface temperatures. Rem. Sens. Environ. 115 (12), 3175–3186.
Shreevastava, A., Bhalachandran, S., McGrath, G.S., et al., 2019. Paradoxical impact of sprawling intra-Urban heat islets: reducing mean surface temperatures while enhancing local extremes. Sci. Rep. 9 (1), 19681.
Simwanda, M., Ranagalage, M., Estoque, R.C., Murayama, Y., 2019. Spatial analysis of surface urban heat islands in four rapidly growing African cities. Remote Sens. 11 (14), 1645.
Sismanidis, P., Bechtel, B., Perry, M., Ghent, D., 2022. The seasonality of surface urban heat islands across climates. Remote Sens. 14 (10), 2318.
Stone, B., Rodgers, M.O., 2001. Urban form and thermal efficiency: how the design of cities influences the urban heat island effect. J. Am. Plann. Assoc. 67 (2), 186–198.
Stone, B., Hess, J.J., Frumkin, H., 2010. Urban form and extreme heat events: are sprawling cities more vulnerable to climate change than compact cities? Environ. Health Perspect. 118 (10), 1425–1428.
United Nations, 2025. World Urbanization Prospects 2025: Summary of Results. United Nations, New York. UN DESA/POP/2025/TR/ NO. 12.
UN-Habitat, 2022. World Cities Report 2022: Envisaging the Future of Cities. United Nations Human Settlements Programme, Nairobi.
Voogt, J.A., Oke, T.R., 2003. Thermal remote sensing of urban climates. Rem. Sens. Environ. 86 (3), 370–384.
Weng, Q., Lu, D., Schubring, J., 2004. Estimation of land surface temperature–vegetation abundance relationship for urban heat island studies. Rem. Sens. Environ. 89 (4), 467–483.
Zhang, W., Derudder, B., 2019. How sensitive are measures of polycentricity to the choice of ‘centres’? A methodological and empirical exploration. Urban Stud. 56 (16), 3339–3357.